NANO LETTERS

Letter

pubs.acs.org/NanoLett

High Purcell Factor Due To Coupling of a Single Emitter to a Dielectric Slot Waveguide

Pavel Kolchin,[†] Nitipat Pholchai,[†,‡] Maiken H. Mikkelsen,[†] Jinyong Oh,[§] Sadao Ota,[†] M. Saif Islam,[§] Xiaobo Yin,[†] and Xiang Zhang*[,†,‡,∥]

[†]NSF Nanoscale Science and Engineering Center (NSEC), University of California, 3112 Etcheverry Hall, Berkeley, California 94720, United States

[‡]Applied Science and Technology Graduate Group, University of California, Berkeley, California 94720, United States

[§]Department of Electrical and Computer EngineeringUniversity of California, 2064 Kemper Hall, Davis, California 95616, United States

[∥]Materials Science Division, Lawrence Berkeley National Laboratory, 1 Cyclotron Road, Berkeley, California 94720, United States

S *Supporting Information*

ABSTRACT: We demonstrate an all-dielectric quantum electrodynamical nanowire-slab system with a single emitter that concentrates the extremely intense light at the scale of 10 × 75 nm^2. The quantum dot exhibits a record high 31-fold spontaneous decay rate enhancement, its optical saturation and blinking are strongly suppressed, and 80% of emission couples into a waveguide mode.

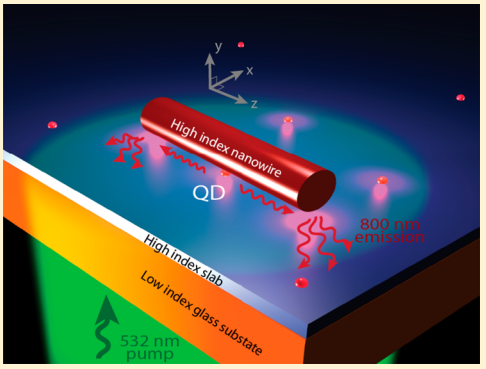

KEYWORDS: *Nanophotonics, quantum dot, field enhancement, emission coupling, all-dielectric waveguide, deep subwavelength light confinement, waveguide QED*

Strong light-matter interactions at the single emitter-photon level are of fundamental importance for quantum information science and constitute the basis of such important applications as quantum memories, switches and gates,[1−8] long-range coupling of single emitters and novel entanglement schemes.[9,10] While narrow microcavity resonances were traditionally used for strong optical interactions,[11,12] subwavelength plasmonic nanostructures have been recently introduced to improve emission directivity and coupling to tightly confined electromagnetic modes,[13−16] enabling strong interaction regime in broadband cavity-free nanoscale one-dimensional environment[2−5] and therefore making it promising as a building block for quantum nanodevices. However, despite significant advances demonstrated by merging plasmonics with quantum optics,[14−16] stronger interaction, high coupling efficiency, and emission rate enhancement have yet to be observed.

We demonstrate here strong optical interactions and emission coupling at single photon and single emitter level using an all-dielectric nanoscale waveguide that exibits a deep subwavelength field confinement of $\lambda^2/50$. The confinement is created by squeezing light in the low index gap region between a high index dielectric nanowire and a slab, where the large discontinuity in the refraction indices concentrates the electric field in the nanometer scale gap region along the nanowire, constituting a deeply confined one-dimensional waveguide mode. Alternative approaches using high-index contrast between dielectric interfaces to overcome the diffraction limit has recently been investigated[19,20] and light concentration at 100 nm scale was demonstrated in a slot waveguide.[20−22] However, incorporating single quantum emitters into such a waveguide while squeezing the active region in order to achieve strong coupling regime remains a challenge.[20]

By placing a single CdSe/ZnS quantum dot (QD) at an optimal position in the system with nanometer precision, enabled by atomic force microscope (AFM) manipulation, we obtain strong spontaneous decay rate enhancement of 31 and strong emission coupling from a single QD into the deeply confined waveguide mode. We observe a high emission coupling efficiency of about 80%. Moreover, we observe that such a strong coupling modifies the emission dynamics: the QD becomes brighter, and its blinking behavior and optical saturation are strongly suppressed. The demonstrated all-dielectric nano-QED system not only achieves simultaneously

Received: October 1, 2014
Revised: November 20, 2014
Published: November 28, 2014

   dx.doi.org/10.1021/nl5037808 | *Nano Lett.* 2015, 15, 464−468

strong field confinement, efficient emission channeling, and enhanced light-matter interactions, but also provides a compact, broad-band, low loss and readily scalable photonic platform for classical and quantum information processing in a one-dimensional continuum.[2−5]

Figure 1a shows the schematic of the all-dielectric nano-QED system that consists of the nanowire-slab waveguide and a single QD strongly coupled to the waveguide mode. In the experiment, the dielectric waveguide is formed by a high-index Si nanowire (refractive index n_1 = 3.7120 + 0.0085i, 260−280 nm in diameter) on top of a 90 nm ZnS film (refractive index n_2 = 2.3). Colloidal CdSe/ZnS core−shell QDs (800 nm peak emission) are spin-coated on the sample to form a disperse monolayer prior to nanowire transfer. The AFM is used for selection and positioning of the nanowires such that a QD is precisely placed right underneath the nanowire. Given the physical size of ∼8 nm of the QDs along with ZnS surface roughness of 6.6 nm (P−V), one creates a nanometer-sized air gap between the nanowires and ZnS film (inset of Figure 1a). Such a narrow nanoscale air gap region along the nanowire supports a deeply confined one-dimensional guided mode. Because of large refactive index contrast the electric field normal to the boundaries jumps up inside the air gap, resulting in high electric energy density concentration in the gap region. Alternatively such a confined mode can be viewed as a cross-coupling between the nanowire waveguide mode and slab mode, resulting in capacitor-like in-phase polarization charge oscillations at the gap boundaries. Because of its capacitor-like electric field distribution inside the gap region, the mode area scales generally as (refractive index)$^{-4}$.[19] Therefore, it is critical to use high index materials in order to increase confinement and Purcell emission rate enhancement.[24] The experimental setup consists of the fluorescence imaging and single photon counting systems with an integrated AFM that allows precision control over the position of individual QDs and nanowires, a major advantage over conventional lithographic approaches with limited lateral resolution. The AFM is operated in tapping mode for topographic imaging while in contact mode for positioning the nanowire on top of the desired QD. At room temperature, the QDs are excited by a 532 nm continuous wave (cw) laser and their fluorescent emission is imaged on a charge-coupled device (CCD) camera (Hamamatsu EM-CCD, C9100). When the QD is placed in the region of large field enhancement, its emission scatters directionally into the waveguide mode and propagates along the waveguide before it scatters out at the ends, indicating the strong interaction between the confined mode and emitter. If necessary, the nanowire is repeatedly repositioned until spatially optimal coupling is observed. A complete description of the experimental setup and AFM manipulation procedures are available in the Supporting Information.

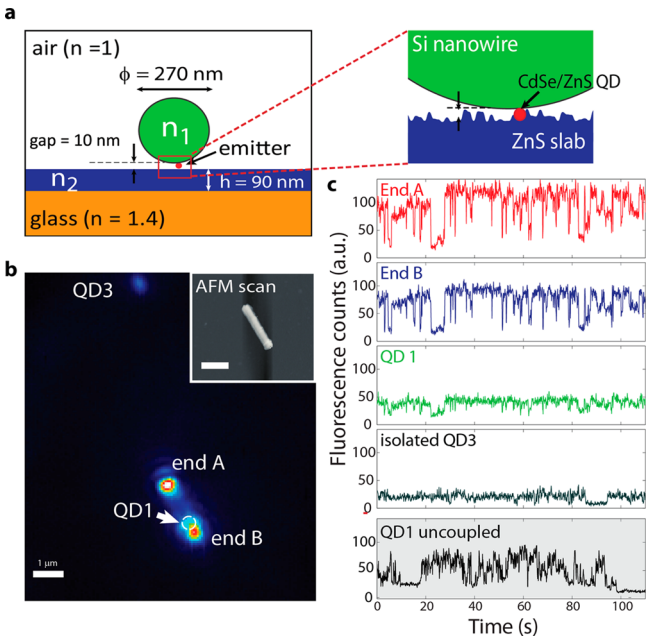

Figure 1. The deep subwavelength all-dielectric QED system with a nanoscale gap. (a) The dielectric nano-QED system consists of the nanowire-slab waveguide and a single quantum emitter strongly coupled to the waveguide mode. Light is confined in the gap region due to the high index contrast for optical modes with dominant electric field components normal to the interfaces. (b) The averaged fluorescence image of a single QD coupled to a nanowire-slab waveguide. The inset shows the AFM scan image of the nanowire. (c) Fluorescence time traces detected at the nanowire ends and at position of the coupled QD1 on the same time axis. Simultaneous blinking of two nanowire ends and coupled QD1 indicates that light from the three spots comes from the same coupled QD1. Time trace of the same QD1 when uncoupled at a different location away from wire is included (shaded) for comparison.

Figure 1b shows the fluorescence image of a single QD that is strongly coupled to the waveguide averaged over 200 s duration. The quantum dot (QD1) is placed underneath the nanowire and the bright glowing ends of the waveguide signify the strong interaction. The intensity time traces from the two ends and from QD1 position reveals fluorescence blinking that is characteristic to a colloidal QD, as shown in Figure 1c. The blinking signal in these three traces are simultaneous (with correlation values higher than 0.9), indicating that the light scattered out at the ends of the waveguide is coming from the same coupled quantum dot (QD1). For comparison, any isolated QD nearby blinks independently (correlation <0.1) from one another and from the coupled QD1.

QD strong interaction with the deeply confined photonic mode is evident as the emission from each nanowire end is about twice as strong as that at QD1 position. The ratio of the fluorescence signals from the two nanowire ends to the sum of all the three spots yields an apparent emission coupling factor of about 80%, which is in good agreement with theoretical prediction of 80% for a Si nanowire on ZnS slab (see Figure 3b). In the meantime, as shown in the final trace (shaded) in Figure 1c, the strong confinement significantly enhances the total photon flux and more than 4 times more photons are collected from coupled QD1 than that of the uncoupled scenario. Moreover, the deep subwavelength confinement is strong enough to achieve near unity emission coupling factor[23,25,26] despite the fact that the colloidal quantum dots are two-dimensional isotropic emitters with random orientation of their crystalline axis.[27]

In order to verify that the emission originates from a single QD emitter, we perform two-photon intensity autocorrelation measurements using a pair of single photon counting modules (SPCMs). Figure 2b shows normalized two-photon intensity correlation $g^{(2)}(\tau)$ of QD2 for both coupled and uncoupled cases. When the emission of the QD is strongly coupled to the waveguide mode, as shown in Figure 2b, the autocorrelations show identical narrow dips measured at the QD position (red curve) and nanowire end (green curve). When uncoupled from

dx.doi.org/10.1021/nl5037808 | Nano Lett. 2015, 15, 464−468

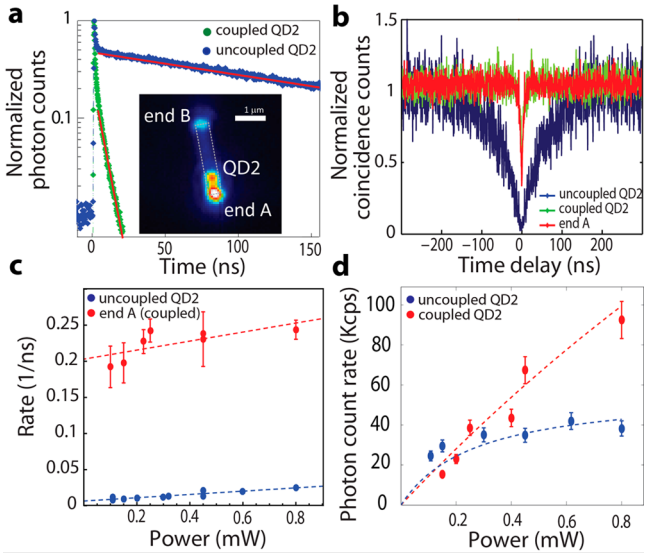

Figure 2. Purcell emission enhancement of a single QD strongly interacting with the deeply confined photonic mode. (a) Direct lifetime measurements of another QD-nanowire system (inset) under pulsed laser excitation shows drastic 31-fold difference from the same QD2 decoupled from the nanowire. (b) Two photon intensity autocorrelation measurements (at pump power 0.45 mW) show antibunching dips confirming single photon emission from the individual quantum emitter. A clear difference in the dip width is observed between the coupled and uncoupled QD, showing a strongly reduced recombination lifetime of the coupled QD. (c) A plot of photon circulation rate is linearly dependent on the pump power. Extrapolation to zero pump value yields the intrinsic lifetime of about 5.2 ± 0.4 ns and 160 ± 22 ns, respectively for the coupled and uncoupled cases, which is in good agreement with the lifetime directly measured under pulsed excitation. (d) Measured total fluorescence peak intensities versus pump power for coupled and uncoupled QD. Dashed lines are fitted to a saturation model. Within the illumination range of the experiment, coupled QD emission remains linear and unsaturated, whereas uncoupled QD clearly saturates at higher pump power.

the nanowire, a much wider dip is measured from the same QD (blue curve). In all three cases $g^{(2)}(0) < 0.5$ verifies that the emission is indeed from a single QD and its single photon state purity is excellently preserved after coupling. Slightly higher value of $g^{(2)}(0)$ for the coupled case is due to spurious uncorrelated fluorescence from the nanowire, finite histogram time-bin size, and dark background photon count rate.

Both lifetime measurements with pulsed excitation and intensity autocorrelation measurement under cw excitation reveal a striking difference in the recombination lifetimes of the coupled and uncoupled QD. Because the emission lifetime varies among different QDs, measurements on the same QD before and after coupling provides unambiguous determination of the Purcell enhancement factor. The pulsed excitation measurements reveal a multiexponential decay curve, characteristic of colloidal QDs (Figure 2a) with a longer time constant corresponding to the radiative recombination lifetime of the bright state.[29] The inset shows the fluorescence image of the strongly coupled QD. A long lifetime of 120−180 ns is typically observed for uncoupled CdSe/ZnS QDs.[30] Extracted from Figure 2a, the recombination lifetimes are 5.4 ± 0.1 ns for the coupled and 170 ± 2 ns for the uncoupled QD, resulting in a strong Purcell enhancement factor of 31 due to the strong field confinement in the deeply confined photonic mode, much greater than observed in plasmonic waveguides and nanoparticles.[14−18,28] This enhancement factor agrees well with the theoretical prediction for a gap of 9 ± 1 nm and corresponds to a field confinement of at least $\lambda^2/50$. Meanwhile, the width of the antibunching dip in intensity autocorrelations (Figure 2b) is determined by the overall emission rates, the sum of the intrinsic decay rate (k_{21}) and the excitation rate (k_{12}), the latter of which is proportional to the pump power. As shown in Figure 2c, extrapolation of the measured emission rates to zero pump power yields the intrinsic lifetimes of 5.2 ± 0.4 and 160 ± 22 ns for the coupled and uncoupled cases, which is in good agreement with the lifetime values directly measured under pulsed excitation.

Importantly, we observe that strong Purcell enhancement tremendously reduces the saturation of the QD bright state emission that is favorable for implementation of high brightness single photon sources. Figure 2d shows peak intensity saturation curves for coupled and uncoupled QD2. The intensity saturation occurs under typical excitation conditions for uncoupled QDs when the excitation rate is higher than the spontaneous emission rate $k_{12} > k_{21}$. However, when QD is coupled to the nanowire the radiative decay rate is significantly enhanced. As a result, the intensity curve shows almost linear dependence on the pump power, indicating the absence of saturation ($k_{12} \ll k_{21}$). The intensity saturation can be also independently determined from the autocorrelation measurements: the relative slope steepness of the rate ($k_{12} + k_{21}$) curve [Figure 2c] indicates the degree of the intensity saturation. Flat curve for the coupled QD indicates that the saturation is tremendously suppressed. For example, under the same excitation power of 0.45 mW, k_{12}/k_{21} = 0.1 and 1.7 for the coupled and uncoupled QD2, respectively. This indicates that for the coupled QD the saturation point ($k_{12} = k_{21}$) should be reached at the pump power of 4.5 mW, 17 times higher than that of the uncoupled QD (0.27 mW). During the period of bright state manifold, the peak photon emission rate (R) of the quantum dot is described by the simple emission model under incoherent pumping $R = \chi k_{12}\, k_{21}/(k_{12}+ k_{21})$.[33−35] The factor χ can be expressed using the emission outcoupling efficiency (γ) into the single mode fiber and the emission quenching factor (k_r/k_{21}) as $\chi = \gamma k_r/k_{21}$. Here k_r is the radiative decay rate from the upper state. By fitting peak intensity saturation curves to this emission model with χ as the only free scaling parameter, we obtain that the saturated peak photon count rate should be 12 times higher for the coupled QD as compared to that of the uncoupled QD. The difference in the saturation photon count factor of 12 and decay enhancement factor of 31 is due to different photon out-coupling efficiencies from QD to microscope objective for coupled (27%) and uncoupled QD (63%) and emission quenching factor of 0.9 for the coupled QD, explained below (see also Supporting Information).

Unambiguous measurements of Purcell effect performed on the same QDs before and after interacting with the deeply confined photonic mode quantitatively confirm the dramatic optical confinement in this waveguide QED system. Theoretical calculation in Figure 3a,b shows how the electric field of the deeply confined photonic modes for 150 and 270 nm diameters, particularly the normal component to the slab, is highly concentrated in the gap region. For 270 nm diameter, a lateral confinement is 75 nm (fwhm), corresponding to an effective mode area of $\lambda^2/50$ at 10 nm gap. As the diameter increases, the second deeply confined photonic mode replaces

dx.doi.org/10.1021/nl5037808 | Nano Lett. 2015, 15, 464−468

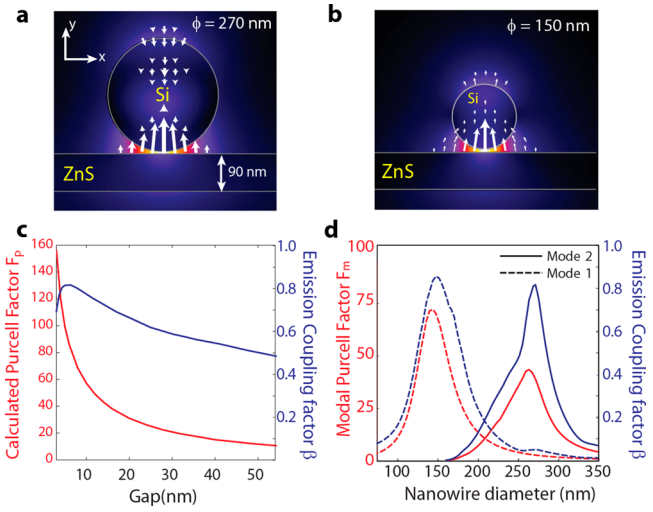

Figure 3. Simulation of Purcell effect. (a,b) The simulated |*E*|-field distribution of the two deeply confined photonic modes shows strong light confinement in the gap region between the nanowire and slab. Arrows indicate *E*-field vectors. The slab thickness is optimized to 90 nm for strongest field confinement. (c) Theoretical total Purcell emission enhancement factor (F_P) and emission coupling factor (β) versus gap size at 270 nm diameter. The curves show strong dependence on the gap size, indicating a tiny gap is crucial for observing the emission enhancement effect. (d) Modal Purcell factor (F_M) at varying nanowire diameter for a fixed 10 nm gap, together with its corresponding coupling factor, reveals the modal structure.

the first one. These modes have different field topology. At 150 and 270 nm, the modes are HE_{11} and HE_{21} circular dielectric waveguide modes,[36] respectively, altered in the proximity of the high index slab. The simulations are performed under the experimental conditions. The theoretical Purcell factor F_P and corresponding coupling factor β for a Si nanowire with 270 nm diameter are shown in Figure 3c with respect to gap size, where an optimally placed linear vertical dipole at the center of the gap region is assumed in the calculation. A tiny gap (below 40 nm) is crucial for observing the emission enhancement effect. Simulation of Purcell effect with varying diameter (Figure 3d) at a fixed gap = 10 nm shows modal structure of the deeply confined photonic modes and confirms that interaction with the second order mode is dominant in our experimental configuration. In particular, because the dipole moment of a colloidal QD is randomly oriented in the plane perpendicular to its crystalline *c*-axis[27] we expect to observe experimentally a Purcell enhancement of at most $F_P/2$ under an optimal condition where the QD *c*-axis is horizontal. The measured Purcell factor of 31 for QD2 therefore corresponds to a theoretical value of 62 or higher at the gap of 9 ± 1 nm consistent with actual geometry of the structure. We also estimate an apparent emission coupling efficiency as 72% for QD2.

More accurate coupling factor estimation takes into account the propagation losses, emission quenching in the nanowire, difference in collection efficiencies at the waveguide ends and at QD position due to different radiation patterns. The objective collection efficiencies, computed from the simulated radiation patterns are 31% for the nanowire end and 40% for the QD out of total out-coupled radiation over full solid angle. The propagation length is estimated as 5.8 ± 2.2 um. The nonradiative rate contribution corresponding to the emission quenching due to ohmic loss in the nanowire is estimated as 10% from fitting intensity saturation curves to the emission model with incoherent pumping (see Supporting Information). With these numbers, the coupling efficiency for QD1 and QD2 of Figures 1-2 become 78% and 71% respectively. These numbers are consistent with 80% value from theory and are hardly affected by 2D orientation averaging due to dominant emission enhancement for *y* dipole component and outperform those for previously reported plasmonic waveguides with coupled single QDs.[14−16] We also note that our waveguide configuration should allow for higher field confinement if higher index materials are used both for the nanowire and slab. For example, for a more ideal Si or transparent GaP nanowire and Si or GaP slab material system and further reduction of gap size to 5 nm the confinement is predicted to be as high as $\lambda^2/300$, corresponding to 91% coupling efficiency (see Supporting Information).

The demonstrated waveguide also substantially improves the QD emission dynamics. Strongly suppressed blinking behavior and enhanced brightness of the QD is observed when coupled to the waveguide. Figure 4 shows fluorescence time traces of

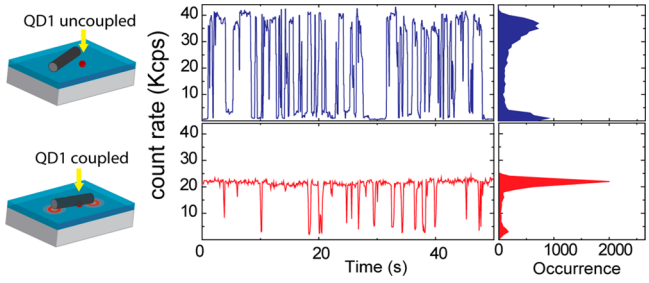

Figure 4. Observation of blinking suppression of the QD coupled to the deeply confined photonic mode. Fluorescence time traces of the QD (left panel) measured at the single photon counters with 100 ms resolution with their corresponding histograms of count rate (right panel). The blinking behavior of coupled QD1 (bottom panel) is strongly suppressed compared to the same QD1 when uncoupled (top panel). The QD is in the bright state 90% of the time when coupled whereas only 63% of the time when uncoupled. This is manifested in a sharp increase in the fraction of bright state emission to the dark state emission in the bottom histogram.

the QD measured at SPCMs with 100 ms resolution. Fluorescence blinking is associated with carrier trapping at surface defects of the QD shell.[31,32] When coupled, the QD is in the bright state 90% of the time, whereas only 63% when uncoupled. The strongly confined waveguide mode accelerates the radiative decay that then competes effectively against the nonradiative transition into the dark state, thereby suppressing the blinking.[32] This blinking suppression, along with the reduction of intensity saturation, results in an increase in total fluorescence.

In conclusion, we demonstrated an all-dielectric waveguide QED system with light concentration at the tens of nanometer scale resulting from a high index contrast dielectrics. The strongly enhanced interaction between the single emitter and deeply confined photonic mode and its effect on the emission dynamics has been observed experimentally with a record high Purcell enhancement factor of 31 in nonresonant photonic systems that is broadband in nature. Such a strong interaction results in strong suppression of QD blinking and optical saturation. The small footprint and broad-band nature of this simple but efficient dielectric system suggests a broader use for

dx.doi.org/10.1021/nl5037808 | *Nano Lett.* 2015, 15, 464−468

efficient on-chip optical components and networks both at classical and quantum level.

■ ASSOCIATED CONTENT

Supporting Information

Experimental setup, procedure of optical coupling via AFM manipulation, characterization of a single emitter using intensity auto-correlation, intensity saturation suppression of the quantum dot coupled to the nanowire, effect of strong emission enhancement on the photon flux, estimation of out-coupling efficiencies, measurement of propagation length of the waveguide, estimation of emission quenching, Estimation of emission coupling factor β, deeply confined photonic modes of the nanowire-slab waveguide, multiemitter interaction regime in the deeply confined photonic waveguide, all localized modes of the nanowire-slab waveguide, effect of waveguide slab thickness on the emission enhancement and confinement, effect of the nanowire background fluorescence on QD intensity saturation, sample preparation method, additional figures, table, and references. This material is available free of charge via the Internet at http://pubs.acs.org.

■ AUTHOR INFORMATION

Corresponding Author

*E-mail: xiang@berkeley.edu.

Author Contributions

P.K., N.P., and M.H.M. contributed equally to this work.

Notes

The authors declare no competing financial interest.

■ REFERENCES

(1) Lvovsky, A. I.; Sanders, B. C.; Tittel, W. *Nat. Photonics* **2009**, *3*, 706−714.
(2) Quan, Q.; Bulu, I.; Loncar, M. *Phys. Rev. A* **2009**, *80*, 011810(R).
(3) Shen, J. T.; Fan, S. *Opt. Lett.* **2005**, *30*, 2001−2003.
(4) Chang, D. E.; Sorensen, A. S.; Demler, E. A.; Lukin, M. D. *Nat. Phys.* **2007**, *3*, 807−812.
(5) Shen, J. T.; Fan, S. *Phys. Rev. Lett.* **2007**, *98*, 153003.
(6) Kojima, K. *Phys. Rev. A* **2003**, *68*, 013803.
(7) Kolchin, P.; Oulton, R. F.; Zhang, X. *Phys. Rev. Lett.* **2011**, *106*, 113601.
(8) Zheng, H.; Gauthier, D. J.; Baranger, H. U. *Phys. Rev. Lett.* **2011**, *107*, 223601.
(9) Martin-Cano, D.; Gonzalez-Tudela, A.; Martin-Moreno, L.; Garcia-Vidal, F. J.; Tejedor, C.; Moreno, E. *Phys. Rev. B* **2011**, *84*, 235306.
(10) Kimble, H. J. *Nature* **2008**, *453*, 1023−1030.
(11) Vahala, K. *Nature* **2003**, *424*, 839−846.
(12) Yoshie, T.; Scherer, A.; Hendrickson, J.; Khitrova, G.; Gibbs, H. M.; Rupper, G.; Ell, C.; Shchekin, O. B.; Deppe, D. G. *Nature* **2004**, *432*, 200−203.
(13) Schuller, J. A.; Barnard, E. S.; Cai, W.; Jun, Y. C.; White, J. S.; Brongersma, M. L. *Nat. Mater.* **2010**, *9*, 193−204.
(14) Akimov, A. V.; Mukherjee, A.; Yu, C. L.; Chang, D. E.; Zibrov, A. S.; Hemmer, P. R.; Park, H.; Lukin, M. D. *Nature* **2007**, *450*, 402−406.
(15) Kolesov, R.; Grotz, B.; Balasubramanian, G.; Stohr, R. J.; Nicolet, A. A. L.; Hemmer, P. R.; Jelezko, F.; Wrachtrup, J. *Nat. Phys.* **2009**, *5*, 470−474.
(16) Huck, A.; Kumar, S.; Shakoor, A.; Andersen, U. *Phys. Rev. Lett.* **2011**, *106*, 096801.
(17) Kinkhabwala, A.; Yu, Z.; Fan, S.; Avlasevich, Y.; Mullen, K.; Moerner, W. E. *Nat. Photonics* **2009**, *3*, 654−657.
(18) Schietinger, S.; Barth, M.; Aichele, T.; Benson, O. *Nano Lett.* **2009**, *9*, 1694−1698.
(19) Robinson, J. T.; Manolatou, C.; Chen, L.; Lipson, M. *Phys. Rev. Lett.* **2005**, *95*, 143901.
(20) Xu, Q.; Almeida, V.; Panepucci, R.; Lipson, M. *Opt. Lett.* **2004**, *29*, 1626−1628.
(21) Creatore, C.; Andreani, L. C.; Miritello, M.; Lo Savio, R.; Priolo, F. *Appl. Phys. Lett.* **2009**, *94*, 103112.
(22) Allen, H. J.; Moore, S. D.; Schmidt, B. S.; Klug, M.; Lipson, M.; Erickson, D. *Nature* **2009**, *457*, 71−75.
(23) Claudon, J.; Bleuse, J.; Malik, N. S.; Bazin, M.; Jaffrennou, P.; Gregersen, N.; Sauvan, C.; Lalanne, P.; Gerard, J. *Nat. Photonics* **2010**, *4*, 174−178.
(24) Purcell, E. M. *Phys. Rev.* **1946**, *69*, 681.
(25) Lund-Hansen, T.; Stobbe, S.; Julsgaard, B.; Thyrrestrup, H.; Sunner, T.; Kamp, M.; Forchel, A.; Lodahl, P. *Phys. Rev. Lett.* **2008**, *101*, 113903.
(26) Lee, K. G.; Chen, X. W.; Eghlidi, H.; Kukura, P.; Lettow, R.; Renn, A.; Sandoghdar, V.; Gotzinger, S. *Nat. Photonics* **2011**, *5*, 166−169.
(27) Empedocles, S. A.; Neuhauser, R.; Bawendi, M. G. *Nature* **1999**, *399*, 126−130.
(28) Kuhn, S.; Haakanson, U.; Rogobete, L.; Sandoghdar, V. *Phys. Rev. Lett.* **2006**, *97*, 017402.
(29) Wu, X.; Sunand, Y.; Pelton, M. *Phys. Chem. Chem. Phys.* **2009**, *11*, 5867−5896.
(30) Shimizu, K. T.; Woo, W. K.; Fisher, B. R.; Eisler, H. J.; Bawendi, M. G. *Phys. Rev. Lett.* **2002**, *89*, 117401.
(31) Frantsuzov, P.; Kuno, M.; Janko, B.; Marcus, R. A. *Nat. Phys.* **2008**, *4*, 519−522.
(32) Shafran, E.; Mangum, B. D.; Gerton, J. M. *Phys. Rev. Lett.* **2011**, *107*, 037403.
(33) Lounis, B.; Bechtel, H. A.; Gerion, D.; Alivisatos, P.; Moerner, W. E. *Chem. Phys. Lett.* **2000**, *329*, 399−404.
(34) Frantsuzov, P.; Marcus, R. A. *Phys. Rev. B* **2005**, *72*, 155321.
(35) Novotny, L.; Hecht, B. *Principles of Nano-Optics*; Cambridge University Press: Cambridge, 2006.
(36) Snitzer, E. *J. Opt. Soc. Am.* **1961**, *51*, 491−498.